Heterogeneous Ice Nucleation in Model Crystalline Porous Organic Polymers: Influence of Pore Size on Immersion Freezing

Lucy Nandy[1], Julie L. Fenton[1], and Miriam Arak Freedman[1,2,*]

1) Department of Chemistry, The Pennsylvania State University, Chemistry Building, University Park, PA 16802, USA
2) Department of Meteorology and Atmospheric Science, The Pennsylvania State University, Chemistry Building, University Park, PA 16802, USA

Revised Manuscript Submitted to The Journal of Physical Chemistry A

[*]Corresponding author: Miriam A. Freedman maf43@psu.edu 814-867-4267, Department of Chemistry, The Pennsylvania State University, 205 Chemistry Building, University Park, PA, 16802, USA.

Abstract

Heterogeneous ice nucleation activity is affected by aerosol particle composition, crystallinity, pore size and surface area. However, these surface properties are not well understood regarding how they act to promote ice nucleation and growth to form ice clouds. Therefore, synthesized materials for which surface properties can be tuned, were examined in immersion freezing mode in this study. To establish the relationship between particle surface properties and efficiency of ice nucleation, materials, here, covalent organic frameworks (COFs), with different pore diameters and degree of crystallinity (ordering) were characterized. Results showed that out of all the highly crystalline COFs, the sample with a pore diameter between 2 and 3 nm exhibited the most efficient ice nucleation activity. We posit that the highly crystalline structures with ordered pores have an optimal pore diameter where the ice nucleation activity is maximized, and that the not highly crystalline structures with non-ordered pores have more sites for ice nucleation. The results were compared and discussed in the context of other synthesized porous particle systems. Such studies give insight on how material features impact ice nucleation activity.

Keywords: heterogeneous ice nucleation, aerosol surface, pore size

Introduction

Earth's climate is altered by ice formation in the atmosphere affecting cloud lifetime and radiative properties.[1,2] Studies to parameterize the ice nucleation of particles have focused on the formation of ice crystals in both cirrus cloud conditions[3–7] and mixed-phase cloud conditions.[8–12] Surface properties of atmospheric aerosol particles that affect the ice nucleating activity are rarely probed systematically. Recent studies to examine how lattice match, functional groups, and defects on the surface resulting from particle aging affect ice nucleation activity have shed some light in understanding ice formation on model aerosol systems.[13–18] Holden and coworkers recently identified active sites at which ice nucleates from supercooled water on macroscopic feldspar substrates using high-speed imaging and suggested that the activity of these sites arises from surface topography and chemistry.[19,20] These surface properties identify as sites for ice nucleation, one of which can consist of pores on a particle surface.

Pores on material surfaces are known to affect heterogeneous ice nucleation activity in immersion mode,[15] condensation mode,[21] as well as deposition mode.[22] However, it has been hypothesized that what we regarded as deposition mode ice nucleation could instead be prior condensation of supercooled water in pores below water saturation and subsequent freezing when ice supersaturation is reached.[23–26] For surface defects, such as, pores, cracks and cavities, pore condensation and freezing has been emphasized in recent studies.[24,27,28] For example, the ice nucleation activity of cloud-processed soot is observed to be enhanced for cirrus cloud conditions by the pore condensation and freezing mechanism due to the increase in pore water compared to unprocessed soot particles.[29] Similarly, aged black carbon soot particles after being oxidized and compacted have also been shown to have improved ice nucleation efficiency,[30] whereas pores

formed in highly fractal particles with more branching features might be too large (> 50 nm) for pore condensation and freezing. Nichman et al. suggested that the pore condensation and freezing mechanism was the major pathway of ice nucleation that occurred in empty spaces or inner pores between black carbon aggregates rather than smaller single aggregates with similar chemistry.[31] In addition, other studies suggest that pore condensation and freezing can take place in pores formed within a single soot aggregate, not only in intra-aggregate pores.[32] Further, it has been demonstrated by Jantsch and Koop that pores between aggregates of spherical particles, like oxidized soot particles formed by freeze-dried water-soluble organics, are suitable to act as sites for ice nucleation.[28]

Synthesized silica particles with uniform pores have been used to study the effect of pore diameter on pore condensation and freezing where it was found that ice nucleation occurred only at temperatures below the homogeneous freezing temperature of pure water (approximately -38 ºC or less).[25,33] Marcolli suggested that pore condensation at water subsaturation and subsequent freezing at temperatures relevant for homogeneous freezing of small volumes of pure water is predominant with respect to heterogeneous freezing triggered by ice active sites within pores.[24] Above the homogeneous freezing temperature of pure water droplets, larger pore volumes (> ~100 nm^3) are required for at least one active site to be present for heterogeneous ice nucleation in water-filled pores.[24] Based on these and subsequent results, the literature has hypothesized that what has traditionally been interpreted as deposition nucleation is actually pore condensation and freezing. Although less common, the heterogeneous freezing events at higher temperatures are assumed to be due to immersion freezing on rare active sites on the pore walls.[24,34]

Whale et al. used carbon nanotubes and graphene oxide sheets as model systems representing carbonaceous particles in the atmosphere to study immersion mode ice nucleation efficiency.[35]

They reported that ice nucleated on the sites inside the nanotube pore walls at higher temperatures than at the edges of the sheets. Further studies have shown how the size of uniform pores in carbon nanotubes affects the ice nucleation activity.[15,36] Both studies have reported ice formation at higher temperatures within pore diameters of 2 – 3 nm due to ice-like cluster formation of a polymorph of ice I, whereas water confined in 1 nm pores had fewer hydrogen bonds, resulting in weaker ice nucleation activity.

In this experimental study, we characterized particle porosity to examine the role of pore size on ice nucleation via immersion freezing. We quantified ice nucleation active site density of crystalline, porous particles that entirely consist of covalent organic frameworks (COFs) as a model system for atmospheric aerosol. Increased interest in emerging porous materials has resulted because of their numerous industrial and environmental applications, including gas adsorption,[37] molecular separation,[38] gas storage,[39] energy storage,[40] catalysis,[41] optoelectronics,[42] and drug delivery.[43] In addition to inorganic porous materials like silica and zeolites, and inorganic-organic porous materials like metal organic frameworks (MOFs), porous organic polymers like COFs have been found to exhibit extraordinary large surface areas (few thousand m^2/g) and are highly stable – both chemically and thermally.[42] Organic aerosols in general, e.g. soot,[44] aged particles coated with organics,[45] secondary organic aerosols,[46] are abundant in the atmosphere and are known to have varied ice nucleation behavior.[47] Freeze-drying of organic aerosol particles can cause changes in particle morphology and can result in solid porous organic particles at high altitudes.[48] Pore sizes in atmospheric aerosol particles can vary from a few Angstroms to up to ~30 nm.[49,50] Chemical functional groups on particle surface and pore walls, like hydroxyl groups, are known to promote ice nucleation[51] by hydrogen bonding with water molecules. In this study, we hypothesize that the ice active sites are due to functional groups in the pore.

COFs are a class of porous organic polymers, which are known for their ability to adsorb water due to high microporosity and various functional groups.[52] Maintaining their porous structures and high surface areas, polar organic functionalities can be incorporated within the COF framework without compromising their stability, which may provide scope for ice nucleation studies. Nevertheless, it is challenging to explore polycondensation reactions to synthesize highly crystalline frameworks with substantial surface area as well as structurally stable ordered pores without collapse.[53] In this paper, COFs are used as a model system to study heterogeneous ice nucleation relevant to freezing behavior in porous organic particles. Imine-based COFs are generally more thermodynamically stable and are generally found as two-dimensional layers.[54–56] To obtain porosity, COFs are synthesized by reacting one monomer (e.g. polyamine) to another complementary functional compound that acts as a linker (e.g. polyaldehyde). Although COFs can be specifically functionalized using a variety of different methods, in this study, we obtained similar COFs, all comprised of benzene rings, imines and aldehydes to form two-dimensional hexagonal networks in order to isolate pore size variability.[57–59] To increase the size of the individual pores, the lengths of the linkers were changed by adding benzene rings to the linear component. However, the increased lengths resulted in non-uniform pore structures during synthesis.[58,60] Here, we studied the effect of increasing pore diameter on ice nucleation efficiency in water-insoluble COFs of both highly crystalline and not highly crystalline structures.

Experimental Methods and Materials

Six hexagonal, imine-linked COF samples were solvothermally synthesized from commercially-available monomers using reported procedures.[58] The pore diameter of each sample was varied by altering the node/linker structure without significantly modifying the hexagonal pore

shape (Figure 1, Table 1). The COFs selected for this study are considered 2D COF structures, i.e., they are covalently polymerized in (approximately) 2D sheets with nanometer-sized periodic hexagonal apertures.[58] The 3D structure of these materials relies on the stacking of the 2D sheets in the third dimension, which is driven by π-π interactions. The 3D pores can be thought of as approximately hexagonal nanotubes, whose diameter is defined by the structure of the 2D sheet. For example, similar to graphene/graphite, a 2D COF contains sp2 planar sheets that are somewhat akin to graphene, and the 3D structure is a stack of these sheets, i.e., graphite. The bonding within the layers is strong and covalent, whereas the bonding between the layers is associative in nature. The COF sheets could stack in several ways: an extreme comparison would be two neighboring sheets whose pores are fully aligned (generating nanotube-like ordering) versus a sheet whose pores are fully blocked by the next sheet beneath it (the next sheet shifted by half of the pore dimension, such that the pore is fully blocked by the next sheet down).[58,61] Our experimental evidence from XRD and BET points to a non-occluded 3D structure with aligned sheets that generate the expected, nanotube-like ordering. This result is consistent with the current consensus in the field for hexagonal 2D COFs without additional functional groups.

All of the samples were characterized by X-ray diffraction (XRD) for crystallinity, the Brunauer–Emmett–Teller (BET) N_2 adsorption method for surface area and pore diameter, and X-ray photoelectron spectroscopy (XPS) for elemental composition. Three samples with high crystallinity and high surface area had uniform and ordered pores of diameter 1.7 nm, 2.7 nm and 3.2 nm. The COF samples with larger pores (4.1 nm and 4.7 nm) had lower crystallinity (and correspondingly, low surface areas), suggesting non-ordering and less uniformity in the samples. Throughout the manuscript, highly crystalline is synonymous to ordered porous COF and not highly crystalline is synonymous to non-ordered porous COF. The crystalline grain size for

assessed samples ranged from 15 nm to 35 nm, based on Scherrer analysis of their XRD patterns. An additional sample ("amorphous COF") was synthesized from the same monomers as the 3.2 nm COF sample (TAPB-$PDA_{crystalline}$), and was deliberately made amorphous (TAPB-$PDA_{amorphous}$) for comparison to the higher-surface area material.[57]

XRD: Powders were front loaded into a silicon zero background holder and diffraction data were collected using a Malvern PANalytical Empyrean III using copper Kα radiation

BET: ~25 mg samples of each COF were prepared for BET analysis by degassing under vacuum for approximately 12 hours at 120 ºC to remove impurities (CO_2, water vapor, organic solvents, etc.), without changing the surface properties or phase of the material. The surface area of the sample was measured using a Micromeritics ASAP 2420 Accelerated Surface Area and Porosity Analyzer. N_2 was used for all adsorption measurements. N_2 isotherms were generated by incremental exposure to nitrogen up to 760 mmHg (1 atm) in a liquid nitrogen (77 K) bath. BET surface areas were calculated from the linear region of the N_2 isotherm at 77 K within the pressure range P/P_0 of 0.05 – 0.09.

XPS: For all the COF samples, XPS experiments were performed using a Physical Electronics VersaProbe III instrument equipped with a monochromatic Al kα x-ray source (hν = 1,486.6 eV) and a concentric hemispherical analyzer. Charge neutralization was performed using both low energy electrons (<5 eV) and argon ions. The binding energy axis was calibrated using sputter cleaned Cu (Cu $2p_{3/2}$ = 932.62 eV, Cu $3p_{3/2}$ = 75.1 eV) and Au foils (Au $4f_{7/2}$ = 83.96 eV) [62]. Peaks were charge referenced to the CH_x band in the carbon 1s spectra at 284.8 eV. Measurements were made at a takeoff angle of 45° with respect to the sample surface plane. This resulted in a typical sampling depth of 3-6 nm (95% of the signal originated from this depth or shallower).

Quantification was done using instrumental relative sensitivity factors (RSFs) that account for the X-ray cross section and inelastic mean free path of the electrons.

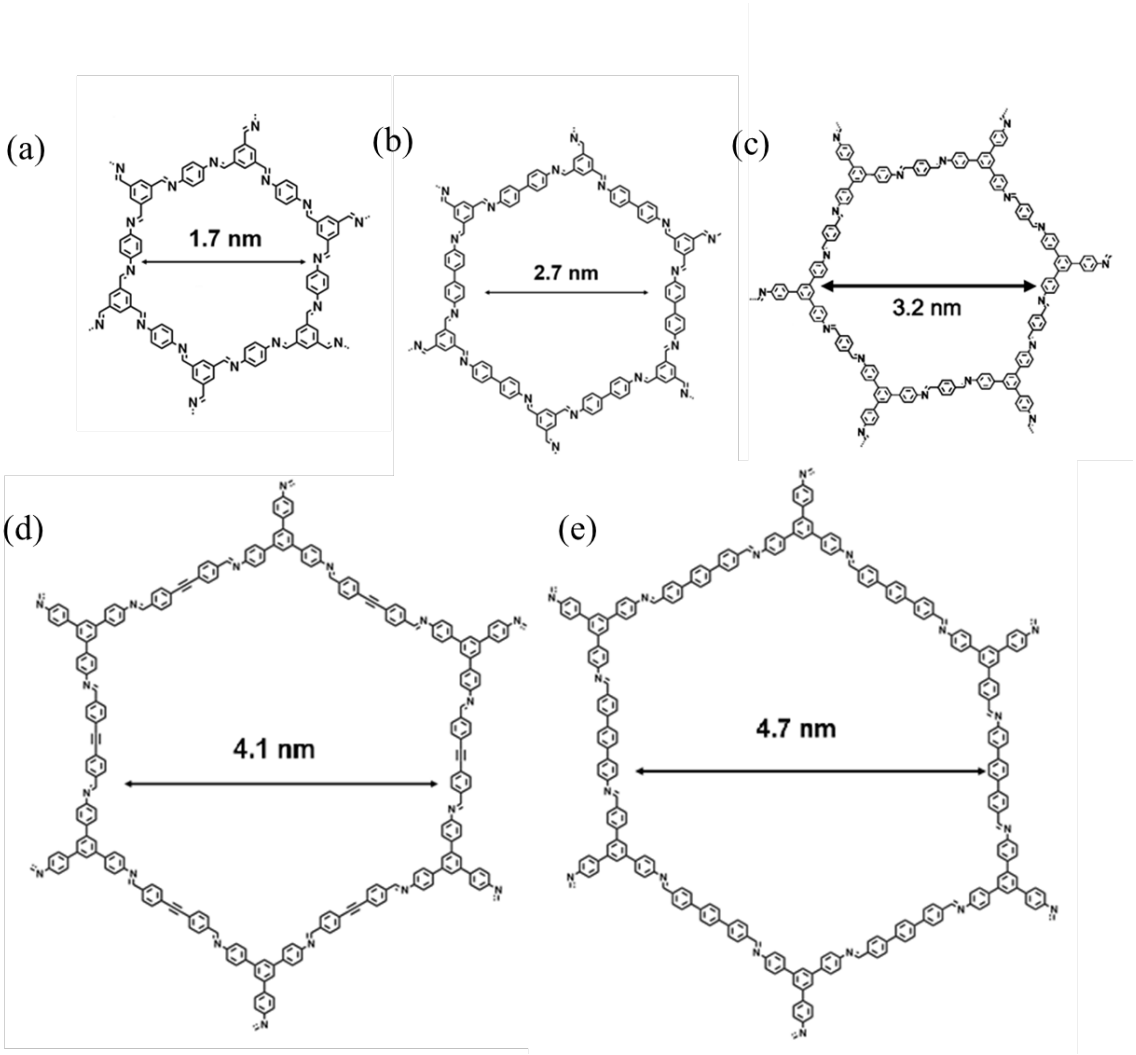

Figure 1. Structures of the crystalline COF materials: (a) DAB-TFB, (b) BND-TFB, (c) TAPB-$PDA_{crystalline}$, (d) TAPB-$PDA_{2\text{-phenyl}}$, and (e) TAPB-$PDA_{3\text{-phenyl}}$.

Table 1. Properties of the COF Samples Used in this Study

COF material[a]	BET surface area (m^2/g)[b]	pore diameter (nm)[b]	O:C (from XPS)[c]
DAB-TFB	1300	1.7	1:40
BND-TFB	2000	2.7	1:13
TAPB-$PDA_{crystalline}$	2800	3.2	1:65
TAPB-$PDA_{amorphous}$	10	1.9	1:70
TAPB-$PDA_{2\text{-phenyl}}$	200	4.1	1:46
TAPB-$PDA_{3\text{-phenyl}}$	100	4.7	1:48

[a]structures are shown in Figure 1.

[b]measured by BET (BET uncertainties range from 0.63 to 6.19% for a standard carbon black material generally used for calibration of the equipment.[63]). Highly crystalline samples with ordered pores have pore diameters 1.7 nm, 2.7 nm, 3.2 nm, and not highly crystalline samples with non-ordered pores have pore diameters 4.1 nm, 4.7 nm. The sample with a pore diameter of 1.9 nm is amorphous in nature.

[c]measured by XPS

Suspensions of individual COF samples were prepared with UHPLC water (Thermo Scientific) at 0.02% w/v and sonicated for 10 – 15 minutes for homogeneous dispersion of the material in water. 2 µL droplets were pipetted onto siliconized glass slides (Hampton Research) and placed in the immersion chamber that is built in-house and described in Alstadt et al.[15] The chamber was cooled by liquid N_2 at a cooling rate of 3 °C/min, and it was constantly purged with N_2 gas to prevent condensation. It is to be noted that due to the large volume of the droplets, evaporation of

the droplets was negligible for the entire duration of the experiment (~ 8 – 10 minutes). Images were taken every 0.5 °C until all the droplets froze completely, and the number of frozen droplets was recorded from each image to calculate the frozen fraction for that temperature (ratio of the number of droplets frozen at a given temperature, *n(T)*, to the total number of droplets, *N*, during the trial. Three to four trials with 36 droplets each were performed for one sample, and the number of surface ice-active nucleation sites was determined at a given temperature per unit surface area (n_s, cm^{-2}) given by

$$n_s(T) = \frac{-ln(1-(n(T)/N))}{V \times C \times SA} \times d$$

where *V* is the volume of the droplet in mL, *C* is the concentration of the particles in g/mL, *SA* is the BET surface area in cm^2/g, and *d* is the dilution factor, here 1.[15,64,65] Trials were also run for ultrapure water droplets to determine their freezing spectrum, referred in this manuscript as background freezing. For all the particle sample trials, the number of nucleation sites per droplet volume was corrected for the background water freezing, i.e., the number of active sites per volume of water is subtracted from the number of active sites per volume of each solution sample, and the standard deviation was calculated for each given temperature.

Results and Discussion

The freezing data for all six COF samples used in this study is shown in Figure 2. The fraction of droplets frozen as a function of temperature in Figure 2a and 2c shows the freezing spectra for the COFs being significantly above that of ultrapure water (background freezing spectra). The freezing spectra for the highly crystalline pore samples in Figure 2a have uniform profiles, with the 2.7 nm pore COF having the warmest profile with an onset temperature of -12.5 ºC. The freezing spectra for the not highly crystalline pore samples in Figure 2c (blue symbols) display a

higher onset temperature for the 4.1 nm pore COF compared to the 4.7 nm sample. The onset temperatures for the crystalline COF samples with pore diameters of 1.7 nm and 4.7 nm were the lowest. The 1.7 nm pore could be too confined for the orientation of water molecules into an ordered ice-like nanocluster, increasing the nucleation barrier to form ice.[36,66] On the other hand, the 4.7 nm pore could be too big, leading to a number of hydrogen bonds in the confined water comparable to that in the bulk water. The onset temperatures for the amorphous COF and the 4.1 nm pore diameter COF (-11.5 ^{o}C and -14 ^{o}C, respectively) were found to be comparable to the 2.7 nm sample although the complete freezing took place at much lower temperatures (-25.5 ^{o}C and -23 ^{o}C) leading to a slope similar to ultrapure water (Figure 2c). The frozen fraction analysis is generally based on the temperatures at which 10%, 50% and 90% (T_{10}, T_{50}, T_{90}) of the droplets are frozen. However, due to the occasional occurrence of one particle that freezes at temperatures higher than the others, the onset temperature is also important as it defines the warmest freezing event. The onset temperatures, T_{10}, T_{50}, T_{90} and the average slopes are reported in Table 2. The slope is calculated by dividing the difference in the percentage frozen (i.e. y-axis of frozen fraction plot times 100) by the difference in the temperature of freezing (i.e. x-axis of frozen fraction plot) and averaging over all data points. The highly crystalline COF samples in Figure 2a had steeper slopes (i.e. larger in absolute value, Table 2) indicating uniform freezing following the freezing onset, whereas the not highly crystalline COF samples in Figure 2c had shallower slopes. These shallower slopes could indicate that the non-uniformity of the active sites leads to complete freezing over a wide range of temperatures. The amorphous COF had the shallowest slope (Figure 2c). The gradual increase in the fraction of frozen droplets per degree of cooling indicates fewer ice active sites at a given temperature compared to highly crystalline samples, and therefore, non-uniform freezing following the freezing onset. It should be noted that the uncertainties in the slopes

for the COF samples with 2.7 nm and 4.1 nm pore diameters are high, and that the slopes may vary depending on experimental set-up, droplet volume and cooling rate. For different experimental parameters, the values of the slope may be different, but the trend will remain the same.

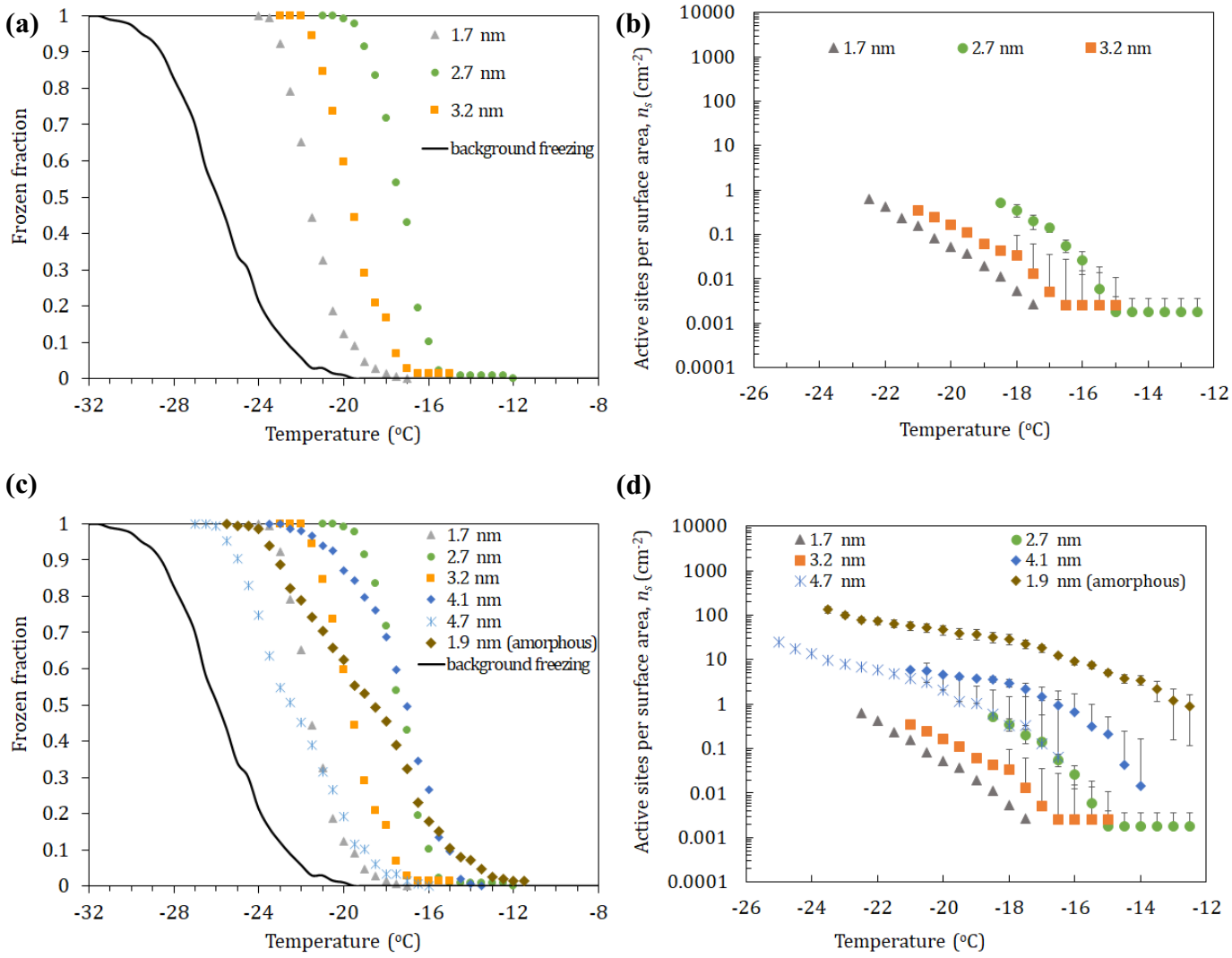

Figure 2. (a) Fraction of droplets frozen as a function of temperature for highly crystalline COF samples. Background freezing of ultrapure water is also shown. (b) Number of active sites frozen for each COF sample per unit surface area as a function of temperature for highly crystalline COF samples. (c) Fraction of droplets frozen as a function of temperature for all systems. (d) Number of active sites frozen as a function of temperature for all systems. The legends on the plot list the

pore diameter. The standard deviations in (b) and (d) could have negative values that cannot be displayed on a logarithmic plot; only the error in the positive direction is shown in most cases. However, the negative values are equivalent to the positive error bars. Some of the uncertainties are small and hidden by the marker.

Table 2. Freezing Temperatures and Average Slopes of the Freezing Spectra of COF Samples

material (pore diameter)[a]	T_{onset} (°C)[b]	T_{10} (°C)	T_{50} (°C)	T_{90} (°C)	slope (%/°C)[c]
pure water	-20.0	-22.8 ± 0.96	-25.9 ± 0.58	-28.6 ± 1.03	-14.7 ± 4.19
DAB-TFB (1.7 nm)	-17.5	-19.9 ± 0.60	-21.6 ± 0.26	-22.9 ± 0.29	-27.3 ± 4.83
BND-TFB (2.7 nm)	-12.5	-16.1 ± 0.32	-17.3 ± 0.37	-18.8 ± 0.56	-31.0 ± 7.13
TAPB-$PDA_{crystalline}$ (3.2 nm)	-15.0	-17.7 ± 0.38	-19.7 ± 0.46	-21.2 ± 0.46	-22.5 ± 0.50
TAPB-$PDA_{amorphous}$ (1.9 nm)	-11.5	-14.7 ± 0.93	-18.9 ± 1.85	-21.5 ± 2.19	-12.1 ± 2.33
TAPB-$PDA_{2\text{-phenyl}}$ (4.1 nm)	-14.0	-15.1 ± 0.27	-17.2 ± 0.66	-19.6 ± 1.48	-19.3 ± 7.00
TAPB-$PDA_{3\text{-phenyl}}$ (4.7 nm)	-16.5	-19.2 ± 0.85	-22.4 ± 1.07	-24.9 ± 0.53	-14.0 ± 0.90

[a]highly crystalline samples are 1.7 nm, 2.7 nm, 3.2 nm, and not highly crystalline samples are 4.1 nm, 4.7 nm.

[b]onset temperatures are reported as determined for all the trials for a single system combined.

[c]experiments were repeated 3 – 4 times (average values are reported within one standard deviation).

The ice nucleation activity is defined based on the ice active site density (n_s), i.e. the most efficient ice nucleation occurs at higher temperatures and larger values as characterized, for example, by T_{50} on the n_s curve (Figure 2b and 2d). The optimum pore diameter for which ice

nucleation activity was the highest was found to be 2.7 nm out of all the highly crystalline samples (Figure 2b), which agrees well with previous freezing studies involving carbon nanotubes.[15,36] However, the ice active site densities for the highly crystalline COF samples were low compared to the not highly crystalline samples (Figure 2d). The ice active site densities for the samples with 4.1 and 4.7 nm pore diameters were the highest out of all the five crystalline samples (Figure 2d). This result could be due to an order of magnitude smaller surface areas as well as non-ordered pore structures when compared to the highly crystalline samples with larger surface areas and more ordering. To explain further: In a highly crystalline COF structure, all polymer-forming monomers make precise bonds in productive directions to form sheets and stack into nanotubes, forming a perfectly regular structure with ordered pores, high apparent crystallinity, and close-to-maximal measured surface area. In a real material, generated by a complex synthetic process, errors in both bond formation and stacking occur, resulting in deviations from the idealized structure.[18,67] These defects could include dangling bonds from unreacted monomers, a higher density of edge ice active sites, unexpected stacking arrangements, and/or different sized pores, though the precise nature of these defects is not easy to directly assess.[61] Structural imperfections impact the extent of crystalline ordering and lower the apparent surface area, making these measurements a reasonable proxy for material quality (and, relatedly, number of defects). Therefore, the larger pore COFs, which exhibit lower crystallinity and lower measured surface area than the smaller pore analogs, likely contain a larger number of structural defects, which may give rise to a greater number of ice active sites per surface area.[68] Supporting this hypothesis further is the fact that the intentionally amorphous COF (which will contain a very high number of structural defects) in Figure 2d has the highest ice active site density of all the samples.[69]

Results from previous pore condensation and freezing studies using clay and silica samples suggest that after water is condensed inside the pores at water subsaturation, at T > -38 °C, heterogeneous ice nucleation can only occur if rare active sites are present within the pores.[24,25,33] In the absence of such ice active sites, ice nucleation within pores via pore condensation and freezing at water subsaturated conditions would not occur at these temperatures. Therefore, ice nucleation may not be dependent on the pore size of the materials at higher temperatures.[33] Note that our study is performed under different conditions (particulate matter in an aqueous droplet) and different temperatures than studies reporting ice formation by pore condensation and freezing. We observed heterogeneous ice nucleation in immersion mode for all the COF samples with pore diameters ranging from 1.7 nm to 4.7 nm indicating presence of active sites. Another explanation of our results could be that ice nucleation is initiated on the external surface of the COF rather than by ice active sites within the pores, yet we found a trend similar to previous studies suggestive of active sites being present in the pores.[15] Alstadt et al. showed similar ice nucleation activities for systems with similar inner pore diameters, where they compared the effect of outer diameter, short lengths, and long lengths of the multiwalled carbon nanotube samples, indicating the importance of inner pore diameters on ice nucleation over outer diameters. The lengths and outer diameters of their samples did not influence the trend in ice nucleation activity. In addition, here, our emphasis is the dependence of ice formation on pore size because the surface chemical functional groups on all the COF samples are the same. Note also, that the surface O:C ratio in all the samples likely does not have a determining effect on ice nucleation activity, as the samples with 1.7, 4.1, and 4.7 nm have similar O:C ratios but different ice nucleation activities. Note, however, that among the highly crystalline samples (1.7, 2.7, and 3.2 nm pores), the surface elemental O:C ratio of the 2.7

nm COF sample is the highest, which may contribute to its higher ice nucleation activity (Table 1).

The COF results compare reasonably well with previous studies of carbon nanotubes that have uniform pore structures with internal pore diameters ranging from 1 nm up to 12 nm.[15] 2 – 3 nm was found to be the optimal pore diameter for ice nucleation to occur in carbon nanotubes as shown in Figure 3. Even though the highly crystalline COF samples have lower ice nucleating activity than the carbon nanotubes, the not highly crystalline COFs have higher ice active site densities. This higher activity of the not highly crystalline COFs results from the lower surface area and increased defects in the not highly crystalline COF samples compared with those of the highly crystalline COFs, resulting in more active sites per unit surface area. It should be noted that the comparison is between two different sets of crystalline materials having similar inner pore size. Overall, it was found that the carbon nanotubes have warmer freezing spectra than the COFs, and both materials have the same optimal pore size that promotes ice nucleation. This narrow range of pore diameter could be optimal for ice nucleation due to abundant hydrogen bonding, compared to fewer hydrogen bonds in smaller and bigger pore diameters.[36] The COF results were also compared to another study with amorphous porous silica with pore sizes of 2 – 11 nm (Figure 3).[70] The silica sample with a pore size of 2.7 nm showed the highest ice nucleation activity at the highest temperatures at which it nucleated ice, supporting our results. Although the pore sizes of the silica samples were similar to the COFs and carbon nanotubes, the ice nucleation activity was seen to be lower than for these systems perhaps because amorphous SiO_2 is a poor ice nucleating material.[70] Note also that the non-ordered porous silica sample (pore size 2 nm) has the lowest ice nucleation activity of any of the silica samples,[70] whereas the COF structures with the most defects have higher ice nucleation activity than the more crystalline COF samples. We expect that this

difference results from the non-ordered porous silica sample being truly amorphous in structure, whereas the not highly crystalline non-ordered porous COF samples have regions of short-range crystalline ordering but are highly defected across longer ranges.[68,69] It is noteworthy to emphasize that the amorphous COF that showed higher ice nucleation activity is actually compared to the ice nucleation activity in COFs that are all crystalline. In contrast, the non-ordered and ordered porous silica are all amorphous, and we have no data for crystalline porous silica to compare with. The finding that both porosity as well as crystallinity are key factors in immersion ice nucleation agrees well with Marak et al. However, they found that amorphous silica was less ice-active than crystalline quartz, whereas for COFs, the amorphous sample was more ice-active.[70] Additionally, in a previous study, crystallinity has been found to play an important role in immersion mode freezing for aluminum hydroxide, alumina, iron oxyhydroxide, and iron oxide samples.[13,14] Moreover, the difference between active sites in amorphous silica and amorphous COF could also be due to different surface chemical groups and different pore structures, not studied here.

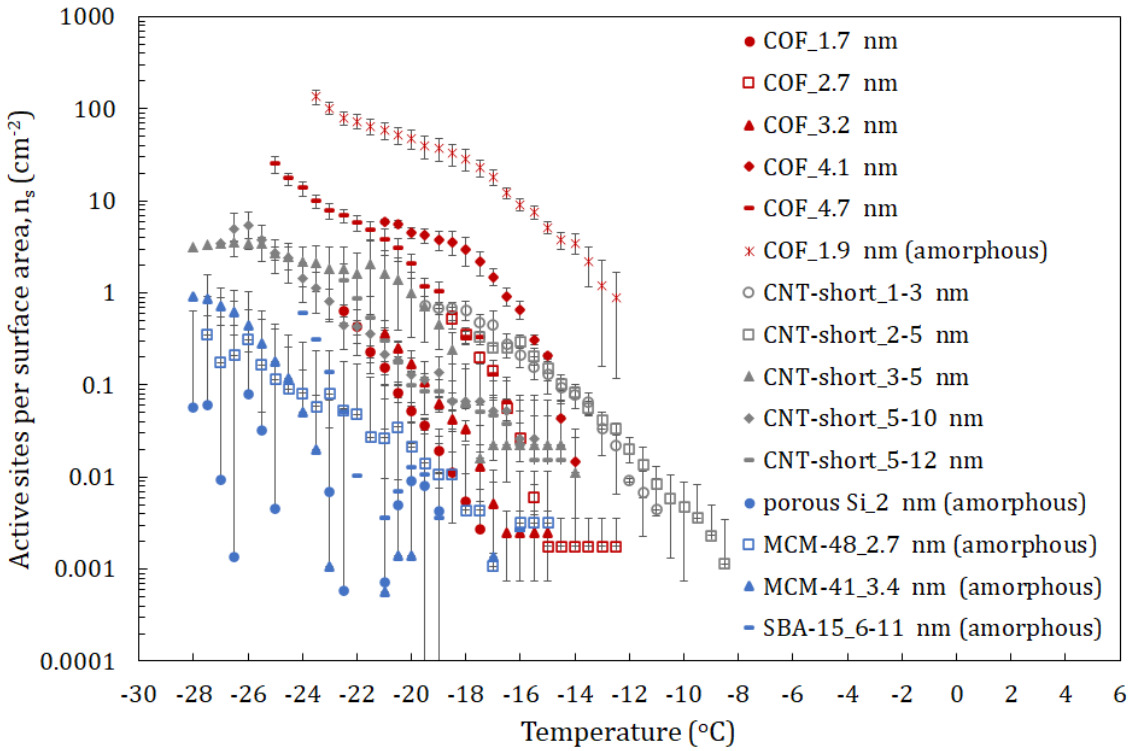

Figure 3. Number of active sites frozen for COF samples (in red), carbon nanotubes (CNT, in grey),[15] amorphous porous silica (in blue)[70] per unit surface area as a function of temperature. Error bars displayed are as described in the Figure 2 caption. Open symbols for each set of materials show the optimal pore diameter between 2 nm and 3 nm for the highest onset temperature. All the COF and multiwalled carbon nanotube samples are crystalline unless noted in the legend.

Conclusions and Atmospheric Implications

Atmospheric aerosols may consist of solid porous organic particles that have diverse surface defects and crystallinity impacting how they cause heterogeneous ice nucleation in clouds via immersion freezing. Therefore, understanding the interaction between the surface of such particles and water at the interface becomes essential. Studying freezing behavior in engineered materials, such as crystalline porous COFs is a useful tool for understanding ice nucleation phenomena due to tunable and controlled pore size, surface chemical functionality, and crystallinity. In this paper, we have investigated the effect of pore diameters between 1.7 nm to 4.7 nm on the ice nucleation efficiency of crystalline COFs, with both high and low crystallinity, in immersion freezing mode. The amorphous COF sample used in this study was synthesized deliberately to compare its ice nucleation activity to that of the crystalline COFs, both high crystallinity and low crystallinity. For the porous COF samples with high crystallinity, the particles with a pore diameter of 2.7 nm showed the highest immersion freezing ice nucleation activity. All the crystalline COF samples with pore diameter less than 2 nm and greater than 3 nm nucleated at lower onset temperatures, although the largest pore size samples with non-ordered pores exhibited higher numbers of active sites. We hypothesize that the increased number of active sites is due to the non-ordered pores and lower surface area rather than the influence of pore size alone. Studies in which single property of the particle is isolated, such as a crystalline vs. amorphous structure or pore size, may provide advanced understanding of the ice nucleation activity of complex aerosol systems. Hydrogen bonding between water and the pore wall could be examined using molecular modeling to provide further insights.

Associated Information

Supporting Information

X-ray diffraction spectra of the crystalline COF samples.

Author Information

Corresponding Author

Email: maf43@psu.edu Phone: 814-867-4267

Notes

The authors declare no competing financial interest.

Acknowledgements

We thank N. Wonderling and J. Shallenberger from the Materials Characterization Lab at the Pennsylvania State University for help with BET and XPS analysis. L. N. and M. A. F. gratefully acknowledge support from NSF grant CHE-1904803. J. L. F. gratefully acknowledges support from the Pennsylvania State University.

References

(1) Seinfeld, J. H. Clouds , Contrails and Climate. *Nature* **1998**, *391*, 837–838.

(2) Seinfeld, J. H.; Bretherton, C.; Carslaw, K. S.; Coe, H.; DeMott, P. J.; Dunlea, E. J.; Feingold, G.; Ghan, S.; Guenther, A. B.; Kahn, R.; et al. Improving Our Fundamental Understanding of the Role of Aerosol-Cloud Interactions in the Climate System. *Proc. Natl. Acad. Sci. U. S. A.* **2016**, *113* (21), 5781–5790. https://doi.org/10.1073/pnas.1514043113.

(3) Kärcher, B.; Lohmann, U. A Parameterization of Cirrus Cloud Formation: Heterogeneous Freezing. *J. Geophys. Res. Atmos.* **2003**, *108*, D14. https://doi.org/https://doi.org/10.1029/2002JD003220.

(4) Hoose, C.; Mohler, O. Heterogeneous Ice Nucleation on Atmospheric Aerosols: A Review of Results from Laboratory Experiments. *Atmos. Chem. Phys.* **2012**, *12*, 9817–9854. https://doi.org/10.5194/acp-12-9817-2012.

(5) Archuleta, C. M.; DeMott, P. J.; Kreidenweis, S. M. Ice Nucleation by Surrogates for Atmospheric Mineral Dust and Mineral Dust/Sulfate Particles at Cirrus Temperatures. *Atmos. Chem. Phys.* **2005**, *5* (10), 2617–2634. https://doi.org/10.5194/acp-5-2617-2005.

(6) Hung, H.-M.; Malinowski, A.; Martin, S. T. Ice Nucleation Kinetics of Aerosols Containing Aqueous and Solid Ammonium Sulfate Particles. *J. Phys. Chem. A* **2002**, *106* (2), 293–306. https://doi.org/10.1021/jp012064h.

(7) Zuberi, B.; Bertram, A. K.; Cassa, C. A.; Molina, L. T.; Molina, M. J. Heterogeneous Nucleation of Ice in (NH4)2SO4-H2O Particles with Mineral Dust Immersions. *Geophys. Res. Lett.* **2002**, *29* (10), 1504.

(8) Atkinson, J. D.; Murray, B. J.; Woodhouse, M. T.; Whale, T. F.; Baustian, K. J.; Carslaw, K. S.; Dobbie, S.; Sullivan, D. O.; Malkin, T. L. The Importance of Feldspar for Ice Nucleation by Mineral Dust in Mixed-Phase Clouds. *Nature* **2013**, *498*, 355–358. https://doi.org/10.1038/nature12278.

(9) Westbrook, C. D.; Illingworth, A. J. Evidence That Ice Forms Primarily in Supercooled Liquid Clouds at Temperatures > −27°C. *Geophys. Res. Lett.* **2011**, *38* (14), L14808. https://doi.org/https://doi.org/10.1029/2011GL048021.

(10) Wilson, T. W.; Ladino, L. A.; Alpert, P. A.; Breckels, M. N.; Brooks, I. M.; Browse, J.; Burrows, S. M.; Carslaw, K. S.; Huffman, J. A.; Judd, C.; et al. A Marine Biogenic Source of Atmospheric Ice-Nucleating Particles. *Nature* **2015**, *525* (7568), 234–238. https://doi.org/10.1038/nature14986.

(11) Murray, B. J.; O'Sullivan, D.; Atkinson, J. D.; Webb, M. E. Ice Nucleation by Particles Immersed in Supercooled Cloud Droplets. *Chem. Soc. Rev.* **2012**, *41* (19), 6519–6554. https://doi.org/10.1039/c2cs35200a.

(12) Field, P. R.; Heymsfield, A. J.; Shipway, B. J.; Demott, P. J.; Pratt, K. A.; Rogers, D. C.; Stith, J.; Prather, K. A. Ice in Clouds Experiment-Layer Clouds. Part II: Testing Characteristics of Heterogeneous Ice Formation in Lee Wave Clouds. *J. Atmos. Sci.* **2012**, *69* (3), 1066–1079. https://doi.org/10.1175/JAS-D-11-026.1.

(13) Chong, E.; Marak, K. E.; Li, Y.; Freedman, M. A. Ice Nucleation Activity of Iron Oxides via Immersion Freezing and an Examination of the High Ice Nucleation Activity of FeO. *Phys. Chem. Chem. Phys.* **2021**, *23* (5), 3565–3573. https://doi.org/10.1039/d0cp04220j.

(14) Chong, E.; King, M.; Marak, K. E.; Freedman, M. A. The Effect of Crystallinity and Crystal Structure on the Immersion Freezing of Alumina. *J. Phys. Chem. A* **2019**, *123* (12), 2447–2456. https://doi.org/10.1021/acs.jpca.8b12258.

(15) Alstadt, V. J.; Dawson, J. N.; Losey, D. J.; Sihvonen, S. K.; Freedman, M. A. Heterogeneous Freezing of Carbon Nanotubes: A Model System for Pore Condensation and Freezing in the Atmosphere. *J. Phys. Chem. A* **2017**, *121* (42), 8166–8175. https://doi.org/10.1021/acs.jpca.7b06359.

(16) Freedman, M. A. Potential Sites for Ice Nucleation on Aluminosilicate Clay Minerals and Related Materials. *J. Phys. Chem. Lett.* **2015**, *6* (19), 3850–3858. https://doi.org/10.1021/acs.jpclett.5b01326.

(17) Primm, K. M.; Schill, G. P.; Veghte, D. P.; Freedman, M. A.; Tolbert, M. A. Depositional Ice Nucleation on NX Illite and Mixtures of NX Illite with Organic Acids. *J. Atmos. Chem.* **2017**, *74* (1), 55–69. https://doi.org/10.1007/s10874-016-9340-x.

(18) Kiselev, A.; Bachmann, F.; Pedevilla, P.; Cox, S. J.; Michaelides, A.; Gerthsen, D.; Leisner, T. Active Sites in Heterogeneous Ice Nucleation-the Example of K-Rich Feldspars. *Science (80-.).* **2017**, *355* (6323), 367–371. https://doi.org/10.1126/science.aai8034.

(19) Holden, M. A.; Whale, T. F.; Tarn, M. D.; Sullivan, D. O.; Walshaw, R. D.; Murray, B. J.; Meldrum, F. C.; Christenson, H. K. High-Speed Imaging of Ice Nucleation in Water Proves the Existence of Active Sites. *Sci. Adv.* **2019**, *5*, 1–10.

(20) Holden, M. A.; Campbell, J. M.; Meldrum, F. C.; Murray, B. J.; Christenson, H. K. Active Sites for Ice Nucleation Differ Depending on Nucleation Mode. *Proc. Natl. Acad. Sci. U. S. A.* **2021**, *118* (18), 1–9. https://doi.org/10.1073/pnas.2022859118.

(21) Umo, N. S.; Wagner, R.; Ullrich, R.; Kiselev, A.; Saathoff, H.; Weidler, P. G.; Cziczo, D. J.; Leisner, T.; Möhler, O. Enhanced Ice Nucleation Activity of Coal Fly Ash Aerosol Particles Initiated by Ice-Filled Pores. *Atmos. Chem. Phys.* **2019**, *19* (13), 8783–8800. https://doi.org/10.5194/acp-19-8783-2019.

(22) Campbell, J. M.; Meldrum, F. C.; Christenson, H. K. Observing the Formation of Ice and Organic Crystals in Active Sites. *Proc. Natl. Acad. Sci.* **2017**, *114* (5), 810–815. https://doi.org/10.1073/pnas.1617717114.

(23) Fukuta, N. Activation of Atmospheric Particles as Ice Nulcei in Cold and Dry Air. *J. Atmos. Sci.* **1966**, *23*, 741–750.

(24) Marcolli, C. Deposition Nucleation Viewed as Homogeneous or Immersion Freezing in Pores and Cavities. *Atmos. Chem. Phys.* **2014**, *14* (4), 2071–2104. https://doi.org/10.5194/acp-14-2071-2014.

(25) David, R. O.; Marcolli, C.; Fahrni, J.; Qiu, Y.; Perez Sirkin, Y. A.; Molinero, V.; Mahrt,

F.; Brühwiler, D.; Lohmann, U.; Kanji, Z. A. Pore Condensation and Freezing Is Responsible for Ice Formation below Water Saturation for Porous Particles. *Proc. Natl. Acad. Sci. U. S. A.* **2019**, *116* (17), 8184–8189. https://doi.org/10.1073/pnas.1813647116.

(26) Christenson, H. K. Two-Step Crystal Nucleation via Capillary Condensation. *CrystEngComm* **2013**, *15* (11), 2030–2039. https://doi.org/10.1039/C3CE26887J.

(27) Campbell, J. M.; Christenson, H. K. Nucleation- and Emergence-Limited Growth of Ice from Pores. *Phys. Rev. Lett.* **2018**, *120* (16), 165701. https://doi.org/10.1103/PhysRevLett.120.165701.

(28) Jantsch, E.; Koop, T. Cloud Activation via Formation of Water and Ice on Various Types of Porous Aerosol Particles. *ACS Earth Sp. Chem.* **2021**, *5*, 604–617. https://doi.org/10.1021/acsearthspacechem.0c00330.

(29) Mahrt, F.; Kilchhofer, K.; Marcolli, C.; Grönquist, P.; David, R. O.; Rösch, M.; Lohmann, U.; Kanji, Z. A. The Impact of Cloud Processing on the Ice Nucleation Abilities of Soot Particles at Cirrus Temperatures. *J. Geophys. Res. Atmos.* **2020**, *125* (3), 1–23. https://doi.org/10.1029/2019JD030922.

(30) Zhang, C.; Zhang, Y.; Wolf, M. J.; Nichman, L.; Shen, C.; Onasch, T. B.; Chen, L.; Cziczo, D. J. The Effects of Morphology, Mobility Size, and Secondary Organic Aerosol (SOA) Material Coating on the Ice Nucleation Activity of Black Carbon in the Cirrus Regime. *Atmos. Chem. Phys.* **2020**, *20* (22), 13957–13984. https://doi.org/10.5194/acp-20-13957-2020.

(31) Nichman, L.; Wolf, M.; Davidovits, P.; Onasch, T. B.; Zhang, Y.; Worsnop, D. R.; Bhandari, J.; Mazzoleni, C.; Cziczo, D. J. Laboratory Study of the Heterogeneous Ice Nucleation on Black-Carbon-Containing Aerosol. *Atmos. Chem. Phys.* **2019**, *19* (19),

12175–12194. https://doi.org/10.5194/acp-19-12175-2019.

(32) Marcolli, C.; Mahrt, F.; Kärcher, B. Soot PCF: Pore Condensation and Freezing Framework for Soot Aggregates. *Atmos. Chem. Phys.* **2021**, *21* (10), 7791–7843. https://doi.org/10.5194/acp-21-7791-2021.

(33) David, R.; Fahrni, J.; Marcolli, C.; Mahrt, F.; Brühwiler, D.; Kanji, Z. The Role of Contact Angle and Pore Width on Pore Condensation and Freezing. *Atmos. Chem. Phys.* **2020**, *20*, 9419–9440. https://doi.org/10.5194/acp-2019-1019.

(34) Marcolli, C. Technical Note: Fundamental Aspects of Ice Nucleation via Pore Condensation and Freezing Including Laplace Pressure and Growth into Macroscopic Ice. *Atmos. Chem. Phys.* **2020**, *20* (5), 3209–3230. https://doi.org/10.5194/acp-20-3209-2020.

(35) Whale, T. F.; Murray, B. J.; O'Sullivan, D.; Wilson, T. W.; Umo, N. S.; Baustian, K. J.; Atkinson, J. D.; Workneh, D. A.; Morris, G. J. A Technique for Quantifying Heterogeneous Ice Nucleation in Microlitre Supercooled Water Droplets. *Atmos. Meas. Tech.* **2015**, *8* (6), 2437–2447. https://doi.org/10.5194/amt-8-2437-2015.

(36) Ohba, T. Size-Dependent Water Structures in Carbon Nanotubes. *Angew. Chemie - Int. Ed.* **2014**, *53*, 8032–8036. https://doi.org/10.1002/anie.201403839.

(37) López-Maya, E.; Montoro, C.; Rodriguez-Albelo, L. M.; Maldonado, C. R. Adsorption Processes on Zeolites and Metal-Organic Frameworks for Industrial and Environmental Applications. In *Zeolites and Metal-Organic Frameworks*; 2019; pp 175–208. https://doi.org/10.2307/j.ctvcmxprm.10.

(38) Fu, J.; Das, S.; Xing, G.; Ben, T.; Valtchev, V.; Qiu, S. Fabrication of COF-MOF Composite Membranes and Their Highly Selective Separation of H2/CO2. *J. Am. Chem. Soc.* **2016**, *138* (24), 7673–7680. https://doi.org/10.1021/jacs.6b03348.

(39) Jia, J.; Chen, Z.; Jiang, H.; Belmabkhout, Y.; Mouchaham, G.; Aggarwal, H.; Adil, K.; Abou-Hamad, E.; Czaban-Jóźwiak, J.; Tchalala, M. R.; Eddaoudi, M. Extremely Hydrophobic POPs to Access Highly Porous Storage Media and Capturing Agent for Organic Vapors. *Chem* **2019**, *5* (1), 180–191. https://doi.org/10.1016/j.chempr.2018.10.005.

(40) Alahakoon, S. B.; Thompson, C. M.; Occhialini, G.; Smaldone, R. A. Design Principles for Covalent Organic Frameworks in Energy Storage Applications. *ChemSusChem* **2017**, *10*, 2116–2129. https://doi.org/10.1002/cssc.201700120.

(41) Bates, J. S.; Bukowski, B. C.; Greeley, J.; Gounder, R. Structure and Solvation of Confined Water and Water-Ethanol Clusters within Microporous Brønsted Acids and Their Effects on Ethanol Dehydration Catalysis. *Chem. Sci.* **2020**, *11* (27), 7102–7122. https://doi.org/10.1039/d0sc02589e.

(42) Bildirir, H.; Gregoriou, V. G.; Avgeropoulos, A.; Scherf, U.; Chochos, C. L. Porous Organic Polymers as Emerging New Materials for Organic Photovoltaic Applications: Current Status and Future Challenges. *Mater. Horizons* **2017**, *4* (4), 546–556. https://doi.org/10.1039/c6mh00570e.

(43) Fang, Q.; Wang, J.; Gu, S.; Kaspar, R. B.; Zhuang, Z.; Zheng, J.; Guo, H.; Qiu, S.; Yan, Y. 3D Porous Crystalline Polyimide Covalent Organic Frameworks for Drug Delivery. *J. Am. Chem. Soc.* **2015**, *137*, 8352−8355. https://doi.org/10.1021/jacs.5b04147.

(44) Adler, G.; Riziq, A. A.; Erlick, C.; Rudich, Y. Effect of Intrinsic Organic Carbon on the Optical Properties of Fresh Diesel Soot. *Proc. Natl. Acad. Sci. U. S. A.* **2010**, *107* (15), 6699–6704. https://doi.org/10.1073/pnas.0903311106.

(45) Jacobson, M. C.; Hansson, H.-C.; Noone, K. J.; Charlson, R. J. Organic Atmospheric

Aerosols: Review and State of the Science. *Rev. Geophys.* **2000**, *38* (2), 267–294. https://doi.org/https://doi.org/10.1029/1998RG000045.

(46) Murray, B. J.; Wilson, T. W.; Dobbie, S.; Cui, Z.; Al-Jumur, S. M. R. K.; Möhler, O.; Schnaiter, M.; Wagner, R.; Benz, S.; Niemand, M.; et al. Heterogeneous Nucleation of Ice Particles on Glassy Aerosols under Cirrus Conditions. *Nat. Geosci.* **2010**, *3* (4), 233–237. https://doi.org/10.1038/ngeo817.

(47) Knopf, D. A.; Alpert, P. A.; Wang, B. The Role of Organic Aerosol in Atmospheric Ice Nucleation: A Review. *ACS Earth Sp. Chem.* **2018**, *2* (3), 168–202. https://doi.org/10.1021/acsearthspacechem.7b00120.

(48) Adler, G.; Koop, T.; Haspel, C.; Taraniuk, I.; Moise, T.; Koren, I.; Heiblum, R. H.; Rudich, Y. Formation of Highly Porous Aerosol Particles by Atmospheric Freeze-Drying in Ice Clouds. *Proc. Natl. Acad. Sci. U. S. A.* **2013**, *110* (51), 20414–20419. https://doi.org/10.1073/pnas.1317209110.

(49) Aylmore, L. A. G.; Quirk, J. P. The Micropore Size Distributions of Clay Mineral Systems. *J. Soil Sci.* **1967**, *18* (1), 1–17. https://doi.org/https://doi.org/10.1111/j.1365-2389.1967.tb01481.x.

(50) Kittaka, S.; Ueda, Y.; Fujisaki, F.; Iiyama, T.; Yamaguchi, T. Mechanism of Freezing of Water in Contact with Mesoporous Silicas MCM-41, SBA-15 and SBA-16: Role of Boundary Water of Pore Outlets in Freezing. *Phys. Chem. Chem. Phys.* **2011**, *13* (38), 17222–17233. https://doi.org/10.1039/C1CP21458F.

(51) Lupi, L.; Hudait, A.; Molinero, V. Heterogeneous Nucleation of Ice on Carbon Surfaces. *J. Am. Chem. Soc.* **2014**, *136* (8), 3156–3164. https://doi.org/10.1021/ja411507a.

(52) Byun, Y.; Je, S. H.; Talapaneni, S. N.; Coskun, A. Advances in Porous Organic Polymers

for Efficient Water Capture. *Chem. - A Eur. J.* **2019**, *25* (44), 10262–10283. https://doi.org/10.1002/chem.201900940.

(53) Liu, R.; Tan, K. T.; Gong, Y.; Chen, Y.; Li, Z.; Xie, S.; He, T.; Lu, Z.; Yang, H.; Jiang, D. Covalent Organic Frameworks: An Ideal Platform for Designing Ordered Materials and Advanced Applications. *Chem. Soc. Rev.* **2021**, *50* (1), 120–242. https://doi.org/10.1039/d0cs00620c.

(54) Slater, A. G.; Cooper, A. I. Function-Led Design of New Porous Materials. *Science* **2015**, *348* (6238), aaa8075. https://doi.org/10.1126/science.aaa8075.

(55) Li, X.; Zhang, C.; Cai, S.; Lei, X.; Altoe, V.; Hong, F.; Urban, J. J.; Ciston, J.; Chan, E. M.; Liu, Y. Facile Transformation of Imine Covalent Organic Frameworks into Ultrastable Crystalline Porous Aromatic Frameworks. *Nat. Commun.* **2018**, *9* (2998), 1–8. https://doi.org/10.1038/s41467-018-05462-4.

(56) Machado, T. F.; Serra, M. E. S.; Murtinho, D.; Valente, A. J. M.; Naushad, M. Covalent Organic Frameworks: Synthesis, Properties and Applications—An Overview. *Polymers (Basel).* **2021**, *13* (970), 1–37. https://doi.org/10.1039/d1qm00015b.

(57) Feriante, C. H.; Jhulki, S.; Evans, A. M.; Dasari, R. R.; Slicker, K.; Dichtel, W. R.; Marder, S. R. Rapid Synthesis of High Surface Area Imine-Linked 2D Covalent Organic Frameworks by Avoiding Pore Collapse During Isolation. *Adv. Mater.* **2020**, *32* (2), 1–5. https://doi.org/10.1002/adma.201905776.

(58) Fenton, J. L.; Burke, D. W.; Qian, D.; Cruz, M. O. D. La; Dichtel, W. R. Polycrystalline Covalent Organic Framework Films Act as Adsorbents, Not Membranes. *J. Am. Chem. Soc.* **2021**, *143* (3), 1466–1473. https://doi.org/10.1021/jacs.0c11159.

(59) Vitaku, E.; Dichtel, W. R. Synthesis of 2D Imine-Linked Covalent Organic Frameworks

through Formal Transimination Reactions. *J. Am. Chem. Soc.* **2017**, *139* (37), 12911–12914. https://doi.org/10.1021/jacs.7b06913.

(60) Geng, K.; He, T.; Liu, R.; Dalapati, S.; Tan, K. T.; Li, Z.; Tao, S.; Gong, Y.; Jiang, Q.; Jiang, D. Covalent Organic Frameworks: Design, Synthesis, and Functions. *Chem. Rev.* **2020**, *120* (16), 8814–8933. https://doi.org/10.1021/acs.chemrev.9b00550.

(61) Evans, A. M.; Strauss, M. J.; Corcos, A. R.; Hirani, Z.; Ji, W.; Hamachi, L. S.; Aguilar-Enriquez, X.; Chavez, A. D.; Smith, B. J.; Dichtel, W. R. Two-Dimensional Polymers and Polymerizations. *Chem. Rev.* **2022**, *122* (1), 442–564. https://doi.org/10.1021/acs.chemrev.0c01184.

(62) Seah, M. P. Summary of ISO/TC 201 Standard: VII ISO 15472 : 2001 — Surface Chemical Analysis — x-Ray Photoelectron Spectrometers — Calibration of Energy Scales. *Surf. Interface Anal.* **2001**, *31*, 721–723.

(63) Badalyan, A.; Pendleton, P. Analysis of Uncertainties in Manometric Gas-Adsorption Measurements. I: Propagation of Uncertainties in BET Analyses. *Langmuir* **2003**, *19* (19), 7919–7928. https://doi.org/10.1021/la020985t.

(64) O'Sullivan, D.; Murray, B. J.; Ross, J. F.; Whale, T. F.; Price, H. C.; Atkinson, J. D.; Umo, N. S.; Webb, M. E. The Relevance of Nanoscale Biological Fragments for Ice Nucleation in Clouds. *Sci. Rep.* **2015**, *5*, 1–7. https://doi.org/10.1038/srep08082.

(65) Vali, G. Quantitative Evaluation of Experimental Results an the Heterogeneous Freezing Nucleation of Supercooled Liquids. *J. Atmos. Sci.* **1971**, *28*, 402–409.

(66) Findenegg, G. H.; Jähnert, S.; Akcakayiran, D.; Schreiber, A. Freezing and Melting of Water Confined in Silica Nanopores. *ChemPhysChem* **2008**, *9* (18), 2651–2659. https://doi.org/10.1002/cphc.200800616.

(67) Friddle, R. W.; Thürmer, K. How Nanoscale Surface Steps Promote Ice Growth on Feldspar: Microscopy Observation of Morphology-Enhanced Condensation and Freezing. *Nanoscale* **2019**, *11* (44), 21147–21154. https://doi.org/10.1039/C9NR08729J.

(68) Nguyen, V.; Grünwald, M. Microscopic Origins of Poor Crystallinity in the Synthesis of Covalent Organic Framework COF - 5. *J. Am. Chem. Soc.* **2018**, *140* (9), 3306−3311. https://doi.org/10.1021/jacs.7b12529.

(69) Smith, B. J.; Overholts, A. C.; Hwang, N.; Dichtel, W. R. Insight into the Crystallization of Amorphous Imine-Linked Polymer Networks to 2D Covalent Organic Frameworks. *Chem. Commun.* **2016**, *52* (18), 3690–3693. https://doi.org/10.1039/c5cc10221a.

(70) Marak, K. E.; Roebuck, J. H.; Chong, E.; Poitras, H.; Freedman, M. A. Silica as a Model Ice-Nucleating Particle to Study the Effects of Crystallinity, Porosity, and Low-Density Surface Functional Groups on Immersion Freezing. *J. Phys. Chem. A* **2022**, *126*, 5965−5973. https://doi.org/10.1021/acs.jpca.2c03063.

TOC graphic: